Second harmonic magnetoacoustic responses of magnetic nanoparticles in magnetoacoustic tomography with magnetic induction[*]

Gepu Guo(郭各朴)[1], Ya Gao(高雅)[1], Yuzhi Li(李禹志)[1], Qingyu Ma(马青玉)[1,†],
Juan Tu(屠娟)[2], and Dong Zhang(章东)[2]

[1] *School of Physics and Technology, Nanjing Normal University, Nanjing 210023, China*
[2] *Institute of Acoustics, Nanjing University, Nanjing 210093, China*

Due to the unique magnetic, mechanical and thermal properties, magnetic nanoparticles (MNPs) have comprehensive applications as the contrast and therapeutic agents in biomedical imaging and magnetic hyperthermia. The linear and non-linear magnetoacoustic responses determined by the magnetic properties of MNPs have attracted more and more attention in biomedical engineering. By considering the relaxation time of MNPs, we derive the formulae of second harmonic magnetoacoustic responses (2H-MARs) for a cylindrical MNP solution model based on the mechanical oscillations of MNPs in magnetoacoustic tomography with magnetic induction (MAT-MI). It is proved that only the second harmonic magnetoacoustic oscillations can be generated by MNPs under an alternating magnetic excitation. The acoustic pressure of the 2H-MAR is proportional to the square of the magnetic field intensity and exhibits a linear increase with the concentration of MNPs. Numerical simulations of the 2H-MAR are confirmed by the experimental measurements for various magnetic field intensities and solution concentrations using a laser vibrometer. The favorable results demonstrate the feasibility of the harmonic measurements without the fundamental interference of the electromagnetic excitation, and suggest a new harmonic imaging strategy of MAT-MI for MNPs with enhanced spatial resolution and improved signal-to-noise ratio in biomedical applications.

Keywords: magnetoacoustic tomography with magnetic induction, second harmonic magnetoacoustic responses, magnetic nanoparticles, magnetic force, mechanical oscillations

PACS: 43.80.Ev, 72.55.+s   **DOI:** 10.1088/1674-1056/ab6843

1. Introduction

Nanoparticles with specific biological properties have been applied to imaging macrophages[1] in human diseases, and *in-vivo* imaging clinical tools are expected to define treatment options and to monitor responses to therapy. Characterized by the quick magnetic response,[2] unique magnetic property,[3] good biological compatibility,[4] low remanence and coercive force, and remarkable specific distribution in a magnetic field, magnetic nanoparticles (MNPs)[5–7] have been widely used as the contrast and therapeutic agents in clinical imaging and magnetic hyperthermia by coating MNPs with appropriate tumor/tissue specific markers[8,9] bounded to the tumor region. Besides the electromagnetic and thermal effects, a great deal of attention has been focused on the magnetoacoustic responses (MARs) of MNPs based on the magnetically induced acoustic oscillations of particles in biomedical tissues. By employing the interaction between the eddy current and the static magnetic field, the new imaging methodology of magnetoacoustic tomography with magnetic induction (MAT-MI)[10–14] was developed to reconstruct the conductivity distribution inside conductive tissues using the Lorentz force induced magnetoacoustic signals. Then, a new imaging technology of MAT-MI incorporating MNPs was pro-

posed by Hu *et al.*[15] and a clear tissue boundary image for the tissue phantom containing superparamagnetic nanoparticles was achieved, demonstrating the feasibility of MNP imaging. By introducing MNPs to MAT-MI under an alternating magnetic excitation,[16] numerical simulations of the electromagnetic and acoustic fields proved that the acoustic sources of MNPs generated by the magnetic forces are much higher than those produced by the Lorentz forces in biological tissues, facilitating potential applications in drug tracing and imaging. A transducer was employed to collect magnetoacoustic signals at the identical frequency of the short-pulse magnetic excitation[17] in MAT-MI. With the impulse response consideration of the transducer, the distribution of MNPs was reconstructed using the MARs collected around the model at the fundamental frequency.

The thermodynamics of electromagnetic energy absorption[18–22] of MNPs was often employed for magnetic hyperthermia in past decades. Kellnberger *et al.*[23] proposed the concept of magnetoacoustic sensing for MNPs and demonstrated the existence of the second harmonics generated in response to a continuous electromagnetic excitation based on the energy absorption of MNPs. The second harmonic magnetoacoustic responses (2H-MARs) were confirmed by acoustic

measurements using a fiber-interferometer detector. Carrey *et al.*[24] derived the expressions of the magnetic force and the vibration velocity of a single MNP based on the calculation of the dissipated power. The behavior of the second harmonic acoustic oscillations was described by analyzing the magnetic force, the magnetic moment, and the magnetic gradient undergone by an MNP during the four quadrants of the simplified rectangular magnetic hysteresis loop. It was reported that the second harmonic mechanical oscillations happened only when the relaxation time of particles was longer than the period of the alternating magnetic field. However, the energy dissipation based magnetoacoustic responses with a long-time continuous magnetic excitation cannot be applied to achieve an acceptable spatial resolution for image reconstruction in MAT-MI. With a short-time alternating magnetic excitation, the behavior of MNPs based on the mechanical vibrations and the corresponding 2H-MAR of an MNP distribution model exhibit great significance in further studies of the monitoring and imaging of MNPs.

In this paper, embarking from the relaxation time of MNPs, the mechanism of the 2H-MAR under an alternating magnetic excitation is investigated based on the mechanical vibrations of particles. The particle velocity of a single MNP with a general complex AC magnetic susceptibility is solved using the differential motion equation by considering the exerted magnetic force. The formulae of the 2H-MAR for a cylindrical MNP solution model is derived based on the principle of MAT-MI. The second harmonic mechanical oscillations of MNPs are demonstrated by the theoretical results of the magnetic force and the corresponding particle velocity. Numerical simulations are verified by the experimental measurements of magnetoacoustic vibrations on the model surface using a laser vibrometer. The acoustic pressure of the 2H-MAR is proved to be proportional to the square of the excitation current (magnetic intensity) with a linear increase with respect to the concentration of the MNP solution. The favorable results demonstrate the feasibility of high-precision second harmonic acoustic measurements without the electromagnetic interference produced by the solenoid, and suggest a new harmonic imaging strategy of MAT-MI for MNPs with enhanced spatial resolution and improved signal-to-noise ratio in biomedical engineering.

2. Principle and method

As shown in Fig. 1, an MNP (radius R_p, volume V_p) positioned in an alternating magnetic field $\boldsymbol{B}$ is subjected to the magnetic force $\boldsymbol{F}_m$ and the viscous force $\boldsymbol{F}_s$ with opposite directions, where $\boldsymbol{F}_s = -6\pi\eta R_p \boldsymbol{u}$, $\boldsymbol{u}$ is the particle velocity and η is the liquid viscosity coefficient of the surrounding medium. Supposing that the coil is excited by a sinusoidal current at the angular frequency ω, the magnetic field intensity is $\boldsymbol{B}(t) = \boldsymbol{B}_0 \cos(\omega t)$ with $\boldsymbol{B}_0 = B_x \boldsymbol{e}_x + B_y \boldsymbol{e}_y + B_z \boldsymbol{e}_z$, where

B_x, B_y and B_z are the magnetic field intensities along the corresponding directions. By treating the MNP as a point dipole,[25] the exerted magnetic force can be approximated by

$$\boldsymbol{F}_m = \mu_0 V_p (\boldsymbol{M} \cdot \nabla) \boldsymbol{H} = V_p (\boldsymbol{M} \cdot \nabla) \boldsymbol{B}, \qquad (1)$$

where ∇ is the Hamilton operator, μ_0 is the permeability of the magnetic field and $\boldsymbol{M}$ is the volumetric magnetization of the MNP. By applying the relationship $\boldsymbol{M} = \chi \boldsymbol{H} = (\chi/\mu_0)\boldsymbol{B}$ with the magnetic susceptibility χ, the magnetic force exerted on the MNP can be rewritten as $\boldsymbol{F}_m = V_p \frac{\chi}{\mu_0} \boldsymbol{B} \cdot \nabla \boldsymbol{B} = \frac{V_p \chi}{2\mu_0} \nabla(\boldsymbol{B}^2)$.[15] Then, by replacing the magnetic moment of the MNP with $\boldsymbol{m} = V_p \boldsymbol{M} = m_x \boldsymbol{e}_x + m_y \boldsymbol{e}_y + m_z \boldsymbol{e}_z$, the exerted magnetic force can be achieved as follows:

$$\begin{aligned} \boldsymbol{F}_m(t) &= (\boldsymbol{m} \cdot \nabla) \boldsymbol{B}_0 \cos(\omega t) \\ &= \left(m_x \frac{\partial \boldsymbol{B}_0}{\partial x} + m_y \frac{\partial \boldsymbol{B}_0}{\partial y} + m_z \frac{\partial \boldsymbol{B}_0}{\partial z} \right) \cos(\omega t). \quad (2) \end{aligned}$$

Since the magnetic field intensities and the corresponding intensity gradients along the x and z direction are much smaller than those along the y direction, equation (3) can be simplified to

$$\begin{aligned} \boldsymbol{F}_m(t) &= m_y \frac{\partial B_y}{\partial y} \cos(\omega t) \\ &= \frac{V_p B_y}{2\mu_0} \frac{\partial B_y}{\partial y} [\chi' + \chi' \cos(2\omega t) + \chi'' \sin(2\omega t)], \quad (3) \end{aligned}$$

where

$$\begin{aligned} m_y(t) &= V_p \mathrm{Re}[(\chi/\mu_0) B_y \exp(i\omega t)] \\ &= (V_p B_y/\mu_0)[(\chi' \cos(\omega t) + \chi'' \sin(\omega t)], \end{aligned}$$

$\chi = \chi' - i\chi''$ is the complex AC susceptibility, $\chi' = \chi_0 / [1 + (\omega\tau)^2]$, $\chi'' = \chi_0 \omega\tau / [1 + (\omega\tau)^2]$,[26,27] χ_0 is the initial susceptibility, τ is the relaxation time of the MNP, and $\mu_0 = 4\pi \times 10^{-7}$ H/m is the permeability of vacuum.

Thus, in order to investigate the motion characteristics of the MNP in the alternating magnetic field $\boldsymbol{B}$ along the y direction, the one-dimensional differential equation of particle motion can be written as

$$m_p \frac{\mathrm{d}u(t)}{\mathrm{d}t} + 6\pi\eta R_p u(t) = F_m(t), \qquad (4)$$

where $u(t)$ and $F_m(t)$ are the particle velocity and the magnetic force along the y direction, $m_p[\mathrm{d}u(t)/\mathrm{d}t]$ represents the inertia force and m_p is the mass of the MNP. By defining $\zeta = 6\pi\eta R_p/m_p$ and $A = \frac{V_p B_y}{2\mu_0} \frac{\partial B_y}{\partial y}$, the differential equation can be solved and the particle velocity is achieved accurately as

$$\begin{aligned} u(t) &= \frac{A\chi'}{\zeta m_p} + \frac{A\chi'}{m_p} \frac{\zeta \cos(2\omega t)}{\zeta^2 + 4\omega^2} \\ &\quad + \frac{A\chi''}{m_p} \frac{\zeta \sin(2\omega t)}{\zeta^2 + 4\omega^2} + \frac{A\chi'}{m_p} \frac{2\omega \sin(2\omega t)}{\zeta^2 + 4\omega^2} \\ &\quad - \frac{A\chi''}{m_p} \frac{2\omega \cos(2\omega t)}{\zeta^2 + 4\omega^2} - \frac{A\chi'}{\zeta m_p} e^{-\zeta t} \\ &\quad - \frac{A\chi'}{m_p} e^{-\zeta t} \frac{\zeta}{\zeta^2 + 4\omega^2} + \frac{A\chi'}{m_p} e^{-\zeta t} \frac{2\omega}{\zeta^2 + 4\omega^2}. \quad (5) \end{aligned}$$

It is clear that the particle velocity is determined by A, χ', χ'', ω and ζ. For the high frequency electromagnetic excitation with $\omega \gg \zeta$, the particle velocity can be simplified to

$$u(t) \approx \frac{A\chi'}{\zeta m_{\mathrm{p}}} + \frac{A\chi'}{m_{\mathrm{p}}}\frac{\sin(2\omega t)}{2\omega} - \frac{A\chi'}{m_{\mathrm{p}}}\frac{\cos(2\omega t)}{2\omega}. \qquad (6)$$

It indicates that the second harmonics of the particle velocity can be generated by the MNP with the velocity decreasing with the excitation frequency. For $\omega \ll \zeta$, the particle velocity can be simplified to

$$u(t) \approx \frac{A\chi'}{\zeta m_{\mathrm{p}}} + \frac{A\chi'}{\zeta m_{\mathrm{p}}}\cos(2\omega t) + \frac{A\chi'}{\zeta m_{\mathrm{p}}}\sin(2\omega t), \qquad (7)$$

which is corresponding to the result used to calculate the dissipated power in Carrey's study for ultrasound therapy.[24] In this study, the averaged particle size of the MNPs is about 110 nm with the parameters of $\tau \approx 1.56 \times 10^{-3}$ s and $\zeta \approx 10^{8}$. Thus, a frequency of the electromagnetic excitation lower than MHz[8] should be selected to assess the characterization of the MNP vibration. Meanwhile, in order to reduce the influence of particle rotation by the alternating magnetic field, the electromagnetic frequency should be much higher than $1/\tau \approx 640$ Hz.[6,24] Under this condition, the particle velocity can be calculated approximately by

$$u(t) \approx \frac{V_{\mathrm{p}}B_y}{12\mu_0\pi\eta R_{\mathrm{p}}}\frac{\partial B_y}{\partial y}[\chi' + \chi'\cos(2\omega t) + \chi''\sin(2\omega t)]. \qquad (8)$$

It shows that, besides the DC component, the mechanical oscillation of the MNP only contains the second harmonic component with the amplitudes determined by χ, B_y and $\partial B_y/\partial y$, which can be worked as the acoustic source in MAT-MI. Under the actions of particle vibrations, the acoustic pressure in biological tissues or fluids obeys[28]

$$\nabla^2 p(\boldsymbol{r}',t) - \frac{1}{c^2}\frac{\partial^2 p(\boldsymbol{r}',t)}{\partial t^2} = \nabla\cdot[\boldsymbol{F}_{\mathrm{m}}(\boldsymbol{r},t)h(\boldsymbol{r})], \qquad (9)$$

where ∇^2 and ∇ are the Laplace and divergence operators, respectively; $p(\boldsymbol{r}',t)$ is the acoustic pressure at $\boldsymbol{r}'$, and c is the acoustic speed. $\nabla\cdot[\boldsymbol{F}_{\mathrm{m}}(\boldsymbol{r},t)h(\boldsymbol{r})]$ is the strength of the acoustic source and $h(\boldsymbol{r})$ is the MNP concentration at $\boldsymbol{r}$. Then, the magnetic force can be written as $\boldsymbol{F}_{\mathrm{m}}(\boldsymbol{r},t) = \boldsymbol{F}_{\mathrm{m}}(\boldsymbol{r})H(t)$, where $\boldsymbol{F}_{\mathrm{m}}(\boldsymbol{r}) = [V_{\mathrm{p}}B_y(\boldsymbol{r})/(2\mu_0)][\partial B_y(\boldsymbol{r})/\partial y]$ is the intensity determined by the magnetic field, and $H(t) = \chi' + \chi'\cos(2\omega t) + \chi''\sin(2\omega t)$ is the 2H-MAR determined by the complex AC susceptibility of the MNP and the time-dependent second harmonics.
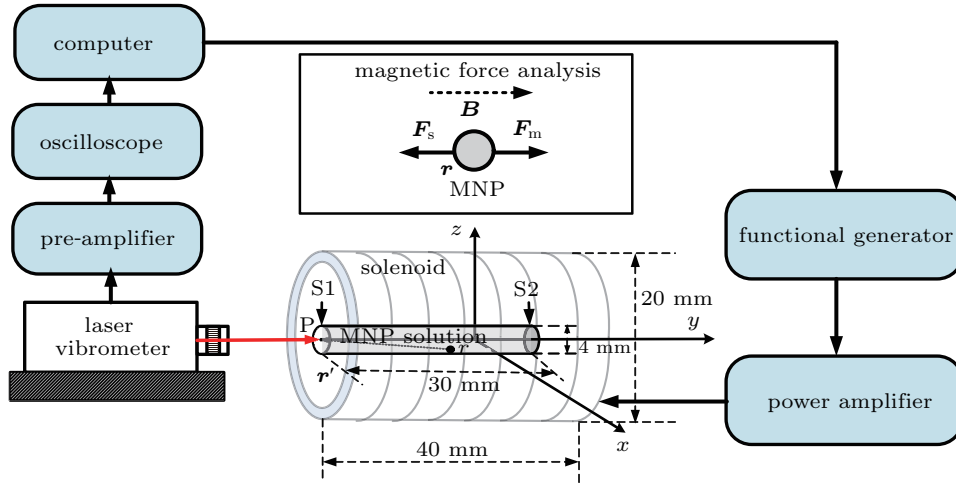

Fig. 1. Schematic diagram of the 2H-MAR measurement system with the inset of magnetic force analysis for a single MNP.

Based on the theory of MAT-MI, the acoustic pressure detected at $\boldsymbol{r}'$ can be calculated by the integral of all the sources inside the solution volume V, and it can be converted to the convolution form by separating the time and space items as follows:[28]

$$\begin{aligned}&p(\boldsymbol{r}',t)\\&= \iiint\limits_V \frac{\nabla\cdot[\boldsymbol{F}_{\mathrm{m}}(\boldsymbol{r})h(\boldsymbol{r})]\otimes\delta(t-|\boldsymbol{r}-\boldsymbol{r}'|/c)}{4\pi|\boldsymbol{r}-\boldsymbol{r}'|}\,\mathrm{d}\boldsymbol{r}\otimes H(t),\,(10)\end{aligned}$$

where $\otimes$ is the convolution operator and $t = |\boldsymbol{r}-\boldsymbol{r}'|/c$ introduces the time delay from $\boldsymbol{r}$ to $\boldsymbol{r}'$. For the acoustic source at $\boldsymbol{r}$, the MNP solution can be decomposed to

$$\begin{aligned}Q(\boldsymbol{r}) &= \nabla\cdot[\boldsymbol{F}_{\mathrm{m}}(\boldsymbol{r})h(\boldsymbol{r})]\\&= h(\boldsymbol{r})\nabla\cdot\left[\frac{V_{\mathrm{p}}B_y(\boldsymbol{r})}{2\mu_0}\frac{\partial B_y(\boldsymbol{r})}{\partial y}\right] + \frac{V_{\mathrm{p}}B_y(\boldsymbol{r})}{2\mu_0}\frac{\partial B_y(\boldsymbol{r})}{\partial y}\nabla h(\boldsymbol{r}).\end{aligned}$$

One can obtain $p(\boldsymbol{r}',t) = p_1(\boldsymbol{r}',t) + p_2(\boldsymbol{r}',t)$, where

$$\begin{aligned}&p_1(\boldsymbol{r}',t)\\&= \iiint\limits_V \frac{h(\boldsymbol{r})\nabla\cdot\left[\frac{V_{\mathrm{p}}B_y(\boldsymbol{r})}{2\mu_0}\frac{\partial B_y(\boldsymbol{r})}{\partial y}\right]\otimes\delta\left(t-\frac{|\boldsymbol{r}-\boldsymbol{r}'|}{c}\right)}{4\pi|\boldsymbol{r}-\boldsymbol{r}'|}\,\mathrm{d}\boldsymbol{r}\otimes H(t)\end{aligned}$$

is the 2H-MAR generated by the inner acoustic sources inside

a homogenous solution with the MNP concentration of $h(\boldsymbol{r})$,

$$
\begin{aligned}
&p_2(\boldsymbol{r}',t) \\
&= \iiint\limits_V \frac{\dfrac{V_{\mathrm{p}}B_y(\boldsymbol{r})}{2\mu_0}\dfrac{\partial B_y(\boldsymbol{r})}{\partial y}\nabla h(\boldsymbol{r}) \otimes \delta\left(t-\dfrac{|\boldsymbol{r}-\boldsymbol{r}'|}{c}\right)}{4\pi|\boldsymbol{r}-\boldsymbol{r}'|}\,\mathrm{d}\boldsymbol{r} \otimes H(t)
\end{aligned}
$$

is the 2H-MAR produced by the boundary acoustic sources between the adjacent solutions with a non-zero $\nabla h(\boldsymbol{r})$. For the proposed cylindrical model with a homogenous MNP solution, the acoustic pressure produced by the boundary sources is much higher than that produced by the inner ones as $p_2(\boldsymbol{r}',t) \gg p_1(\boldsymbol{r}',t)$,[29] and the acoustic pressure of the 2H-MAR can be described by

$$
p(\boldsymbol{r}',t) = p_2(\boldsymbol{r}',t) = p_\delta(\boldsymbol{r}',t) \otimes H(t), \tag{11}
$$

where

$$
p_\delta(\boldsymbol{r}',t) \approx \iiint\limits_V \frac{Q_1(\boldsymbol{r}) \otimes \delta(t-|\boldsymbol{r}-\boldsymbol{r}'|/c)}{4\pi|\boldsymbol{r}-\boldsymbol{r}'|}\,\mathrm{d}\boldsymbol{r}
$$

can be considered as the impulse response of the cylindrical solution model under the electromagnetic excitation of an ideal Dirac function, and

$$
Q_1(\boldsymbol{r}) = \frac{V_{\mathrm{p}}B_y(\boldsymbol{r})}{2\mu_0}\frac{\partial B_y(\boldsymbol{r})}{\partial y}\nabla h(\boldsymbol{r})
$$

is the strength of the boundary acoustic source at $\boldsymbol{r}$.

3. Numerical simulation

To establish an alternating magnetic field with a high intensity, a solenoid was fabricated with the turns, length and diameter of 300, 40 mm and 20 mm, respectively. By measuring the inductance (1.2 mH) and the resistance (4.7 Ω) of the solenoid using an impedance analyzer (Agilent 4294 A, Agilent Technologies, USA), a resonant circuit at the frequency of 4.86 kHz was designed, which satisfies the frequency requirements for Eq. (8). Distributions of the magnetic field intensity and the corresponding intensity gradient as well as the product of $B_y(\boldsymbol{r})\left[\partial B_y(\boldsymbol{r})/\partial y\right]$ were simulated at the peak current of 6 A. A simplified cylinder MNP solution model with the length of 30 mm and the radius of 2 mm was designed, and the center point P on the left surface of the model was set as the observation position to analyze the 2H-MAR of the system. The concentration of the MNP solution was set to 30 mg/ml with $\eta = 8.9 \times 10^{-4}$ Pa·s, $\tau = 1.56 \times 10^{-3}$ s, $\chi_0 = 0.58$, $\chi' = 1.93 \times 10^{-4}$, $\chi'' = 1.06 \times 10^{-2}$ at 4.86 kHz. Then, with the simulation of the impulse response $p_\delta(P,t)$ at the observation point P, the 2H-MAR of $p(P,t)$ under the sinusoidal magnetic excitation was achieved.

By integrating all the sources inside the entire MNP solution model, the impulse responses produced by the boundary and inner acoustic sources are illustrated in Fig. 2. It shows

that the acoustic pressure of the 2H-MAR generated by the boundary MNPs is much higher than that produced by the inner ones, and the acoustic pressures generated by the MNPs on the left surface (S1) of the model are much higher than those produced by the MNPs on the right one (S2). Meanwhile, the acoustic pressure generated by inner MNPs is very weak due to the low-level $\nabla h(\boldsymbol{r})$ inside the uniform solution. Further, by considering the sinusoidal magnetic excitation, the 2H-MAR with the maximum pressure of about 0.12 Pa is achieved as shown in inset (a) and only one peak at 9.72 kHz is clearly displayed in the corresponding spectrum in inset (b), confirming the existence of the second harmonic oscillations.
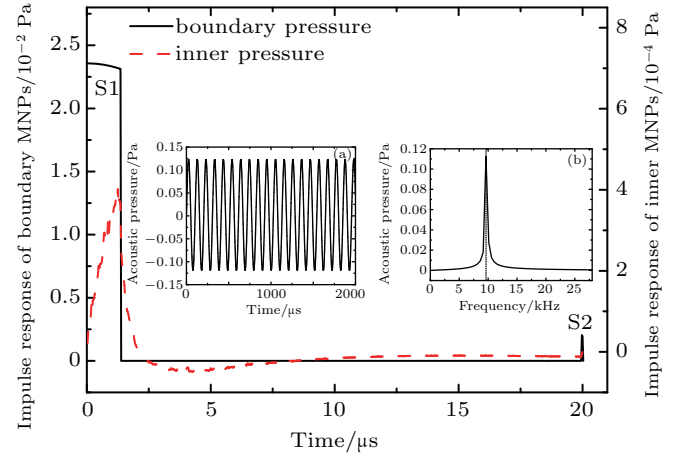

Fig. 2. Impulse responses of the boundary and inner MNPs with the insets of (a) the 2H-MAR and (b) the corresponding spectrum under a sinusoidal magnetic excitation.

In order to optimize the 2H-MAR of the system, pressure dependences of the magnetic field intensity and the concentration of MNPs on $p(P,t)$ are conducted. By fixing the left surface (S1) at $y = -20$ mm as shown in Fig. 1, the magnetic field intensity dependence of $p(P,t)$ is simulated by increasing the excitation current from 1.5 A to 6.5 A, as shown by black circles in Fig. 3(a). The distribution shows a linear proportion to the square of the excitation current, which gives a further verification to $B_y(\boldsymbol{r})\left[\partial B_y(\boldsymbol{r})/\partial y\right]$ of the 2H-MAR with a fixed $\nabla h(\boldsymbol{r})$. Meanwhile, numerical distributions of the 2H-MAR for the solution model in Fig. 3(b) (black circles) exhibit a linear increase tendency with respect to the concentration C of MNPs.

As shown in Fig. 1, the experimental magnetoacoustic measurement system was established using the laser vibrometer (Polytec OFV-503, Polytec Company, German) to verify the 2H-MAR of the MNP solution model in an alternating magnetic field. A functional generator (Agilent 33220 A, Agilent Technologies, USA) was used to send out a 10-cycle sinusoidal waveform at the resonant frequency of 4.86 kHz with the pulse repetition frequency (PRF) of 50 Hz. The tone-burst signal was amplified by the constant-current power supply (HEA-500 G, Foneng, China) to drive the home-made solenoid. A reflective polyethylene terephthalate (PET) membrane with a thickness of 5 μm was stick on the center of the

left surface of the MNP solution model to transmit the acoustic vibrations[30] from the inside MNPs. To achieve a stable interference output, the laser sensor was adjusted to ensure the light beam perpendicular to the reflective membrane. The waveform output of the laser sensor was amplified by the low-noise amplifier (46 dB, NF SA-230F5, Japan) and collected by a digital oscilloscope (Agilent DSO9064A, Agilent Technologies, USA) with DC filtering. The accurate magnetoacoustic vibration displacement was calibrated by the displacement-voltage relationship of the laser sensor. In MNP fabrication, a modified polyol method[7] was employed to synthesize the Fe_3O_4 nanoparticles. In a typical experiment, $FeCl_3 \cdot 6H_2O$ (1.65 g) and trisodium citrate (0.75 g) were dissolved in ethylene glycol (50 ml). Then sodium acetate (NaAc, 3 g) was dropped into the above solution under stirring. The obtained yellow solution was then transferred into a Teflon-lined stain-less-steel autoclave and heated at 200 °C for 10 h. Then, the autoclave was naturally cooled down to room temperature. The acquired black precipitates were washed with deionized water and ethanol three times. Thus, the MNPs with the center size of about 110 nm was fabricated to conduct the experiment of the 2H-MAR.
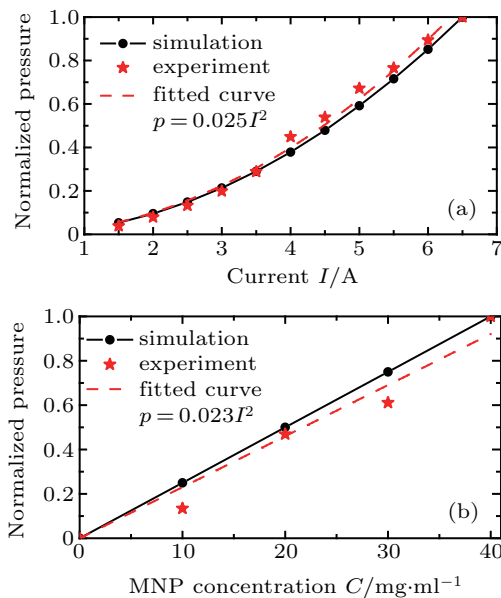

Fig. 3. Acoustic pressure distributions of the 2H-MAR with respect to (a) the excitation current and (b) the concentration of the cylindrical MNP solution model.

The experimental vibration displacement of the model with the concentration of 30 mg/ml at $I = 6$ A is illustrated in Fig. 4 with the corresponding spectrum presented in inset (a). Under the excitation of a 10-cycle burst signal, the resonant current as shown in inset (b) is produced by the solenoid at the frequency of 4.86 kHz. The cycles of the magnetoacoustic vibration are double as shown in Fig. 4, and the 2H-MAR of the MNP solution model is also verified by the only peak at 9.72 kHz, which is consistent well with the theoretical results as presented in Fig. 2. By differentiating the vibration displacement, the estimated acoustic pressure of about 0.6 Pa is

consistent qualitatively with the simulated result. The higher acoustic pressure may be produced by the size, aggregation and magnetization characteristics of the experimental MNPs. For the experimental configuration as shown in Fig. 1, acoustic pressures are measured by increasing the driving current from 1.5 A to 6.5 A with a step of 0.5 A, as plotted in Fig. 3(a) by red stars. Applying the quadratic fitting, the fitted curve for the experimental data is achieved as $p = 0.025I^2$, which shows a good agreement with the theoretical and numerical results. Then, by adjusting the concentration of the MNP solution model, the acoustic pressure distribution with respect to the concentration is measured as illustrated in Fig. 3(b). Similar to the numerical simulations, a linear relationship of $p = 0.023C$ is obtained as the fitted line, which is beneficial to the potential applications of concentration imaging for MNPs based on the 2H-MAR in MAT-MI.
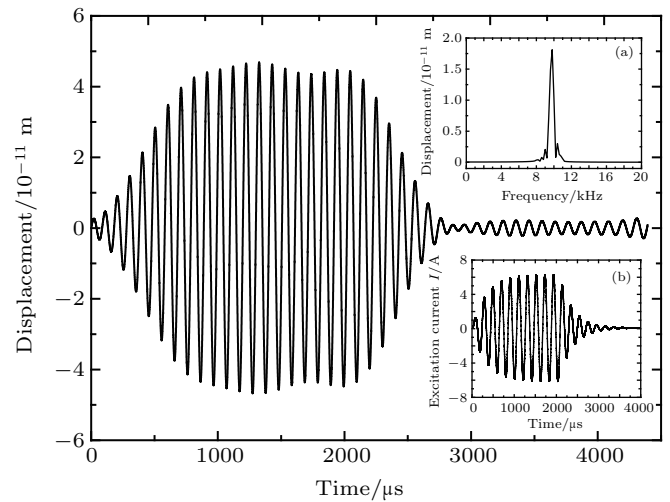

Fig. 4. Magnetoacoustic vibration displacement of the 2H-MAR after DC filtering with the inset (a) of the corresponding spectrum and the inset (b) of the 10-cycle excitation current.

4. Discussion

In the previous study of Kellnberger et al.,[23] the internal energy of MNPs evoked by a continuous electromagnetic excitation was derived to describe the power dissipation, and the appearance of the second harmonic magnetoacoustic resonance was theoretically demonstrated. However, except for the energy absorption of medium magnetization in the period of an alternating magnetic field, the 2H-MAR of the MNP solution model in terms of the shape and size was not taken into account, which might introduce significant influences on magnetoacoustic measurement and image reconstruction with the long-time continuous alternating magnetic excitation in MAT-MI. By considering the second harmonic mechanical oscillations and the integral effects of all MNPs with a short-time pulsed high-frequency magnetic excitation in our study, the structure characteristics of the solution model can be extracted from the 2H-MAR to reconstruct the distribution of MNPs. Meanwhile, the acoustic pressure of the 2H-MAR is much

higher than that produced by a single MNP, which is easy to be verified by experimental measurements.

For the MAT-MI studies carried out by Hu and He[15] and Mariappan *et al.*,[17] magnetoacoustic signals generated by superparamagnetic iron oxide nanoparticles were collected around the phantom by a transducer at the fundamental frequency (0.5 MHz) of the short-time pulsed magnetic excitation, which might be caused by the experimental factors stated in the following. The relaxation time of the superparamagnetic nanoparticles was much smaller than the period of the alternating magnetic field, only mechanical vibrations at the fundamental frequency of the electromagnetic excitation could be produced by the magnetizations of MNPs. Meanwhile, due to the narrow bandwidth of the transducer (TRS ceramic, peak frequency 0.5 MHz, bandwidth 60%),[17] only the fundamental component around 0.5 MHz could be detected for image reconstruction. Nevertheless, the pilot investigations on MAT-MI with MNPs can still provide a solid experimental basis for the harmonic imaging of MAT-MI based on the 2H-MAR of MNPs.

The 2H-MAR of MNPs is demonstrated by theoretical simulations and experimental measurements, and only the second harmonic mechanical oscillations are detected by the laser vibrometer in our study. However, due to the linear and nonlinear electromagnetic interference of the coil, the 2H-MAR of MNPs may be influenced by the mechanical vibrations at the fundamental and the second harmonic frequencies. In order to reduce the interference between the electromagnetic excitation and the magnetoacoustic measurements in practical applications, an accurate sinusoidal excitation should be applied to minimize the second-harmonic electromagnetic excitation and a narrow bandwidth transducer with the central frequency at the second-harmonic frequency should be used to detect the 2H-MAR of MNPs. In addition, the systems of the electromagnetic excitation and the magnetoacoustic measurement should be fixed on two damping platforms to block the mutual interference of mechanical vibrations.

5. Conclusion

In conclusion, embarking from the relaxation time of MNPs, the mechanism of magnetoacoustic oscillations under an alternating magnetic excitation is investigated based on mechanical effects. The 2H-MAR of a cylindrical MNP solution model is derived using the principle of MAT-MI. Numerical simulations and experimental measurements of magnetoacoustic vibration using a laser vibrometer prove that only the second harmonic magnetoacoustic vibrations of MNPs can be generated by the exerted magnetic force due to the interaction

of the alternating magnetic field intensity and the corresponding intensity gradient. The acoustic pressure of the 2H-MAR is proportional to the square of the magnetic field intensity and exhibits a linear increase with the concentration of the MNP solution. The favorable results demonstrate the feasibility of magnetoacoustic measurements at the second harmonic frequency without the fundamental interference of the electromagnetic excitation, and suggest a new harmonic imaging strategy of MAT-MI for MNPs with enhanced spatial resolution and improved signal-to-noise ratio in biomedical applications.

References

[1] Weissleder R, Nahrendorf M and Pittet M J 2014 *Nat. Mater.* **13** 125
[2] Cabrera D, Coene A, Leliaert J, Artés-Ibáñez E J, Dupré L, Telling N D and Teran F J 2018 *ACS Nano* **12** 2741
[3] Li Q, Kartikowati C W, Horie S, Ogi T, Iwaki T and Okuyama K 2017 *Sci. Rep.* **7** 9894
[4] Chi Q, Ma T, Dong J, Cui Y, Zhang Y, Zhang C, Xu S, Wang X and Lei Q 2017 *Sci. Rep.* **7** 3072
[5] Oh J, Feldman M D, Kim J, Condit C, Emelianov S and Milner T E 2006 *Nanotechnology* **17** 4183
[6] Usov N A and Liubimov B Y 2012 *J. Appl. Phys.* **112** 023901
[7] Chaughule R S, Purushotham S and Ramanujan R V 2012 *Proc. Natl. Acad. Sci. India Sect. A: Phys. Sci.* **82** 257
[8] Steinberg I, Ben-David M and Gannot I 2012 *Nanomed.: NBM* **8** 569
[9] Kalambur V S, Han B, Hammer B E, Shield T W and Bischof J C 2005 *Nanotechnology* **16** 1221
[10] Xia R, Li X and He B 2007 *Appl. Phys. Lett.* **91** 083903
[11] Mariappan L, Li X and He B 2011 *IEEE Trans. Biomed. Eng.* **58** 713
[12] Sun X, Zhang F, Ma Q, Tu J and Zhang D 2012 *Appl. Phys. Lett.* **100** 024105
[13] Yu Z, Dai S, Ma Q, Guo G, Tu J and Zhang D 2018 *IEEE Trans. Biomed. Eng.* **65** 2512
[14] Li X, Yu K and He B 2016 *Phys. Med. Biol.* **61** R249
[15] Hu G and He B 2012 *Appl. Phys. Lett.* **100** 013704
[16] Yan X, Zhang Y and Liu G 2018 *Chin. Phys. B* **27** 104302
[17] Mariappan L, Shao Q, Jiang C, Yu K, Ashkenazi S, Bischof J C and He B 2016 *Nanomed.: NBM* **12** 689
[18] Laurent S, Dutz S, Häfeli U O and Mahmoudi M 2011 *Adv. Colloid Interface Sci.* **166** 8
[19] Derfus A M, von Maltzahn G, Harris T J, Duza T, Vecchio K S, Ruoslahti E and Bhatia S N 2007 *Adv. Mater.* **19** 3932
[20] Stanley S A, Gagner J E, Damanpour S, Yoshida M, Dordick J S and Friedman J M 2012 *Science* **336** 604
[21] Feng X, Gao F and Zheng Y 2013 *Appl. Phys. Lett.* **103** 083704
[22] Piao D, Towner R A, Smith N and Chen W R 2013 *Med. Phys.* **40** 063301
[23] Kellnberger S, Rosenthal A, Myklatun A, Westmeyer G G, Sergiadis G and Ntziachristos V 2016 *Phys. Rev. Lett.* **116** 108103
[24] Carrey J, Connord V and Respaud M 2013 *Appl. Phys. Lett.* **102** 232404
[25] Cao Q, Han X and Li L 2012 *J. Phys. D: Appl. Phys.* **45** 465001
[26] Xiang Q, Zhong J, Zhou M, Cesar P and Liu W 2011 *J. Appl. Phys.* **109** 07B317
[27] Mamiya H and Jeyadevan B 2011 *Sci. Rep.* **1** 157
[28] Zhou Y, Wang J, Sun X, Ma Q and Zhang D 2016 *J. Appl. Phys.* **119** 094903
[29] Guo G, Ding H, Dai S and Ma Q 2017 *Chin. Phys. B* **26** 084301
[30] Tao C, Guo G, Ma Q, Tu J, Dong Z and Hu J 2017 *J. Appl. Phys.* **122** 014901